Mechanism of Human *S*-Adenosylmethionine Decarboxylase Proenzyme Processing As Revealed by the Structure of the S68A Mutant[†,‡]

William D. Tolbert,[§] Yang Zhang,[§] Sarah E. Cottet,[§] Eric M. Bennett,[§] Jennifer L. Ekstrom,[§] Anthony E. Pegg,[||] and Steven E. Ealick*[,§]

Department of Chemistry and Chemical Biology, Cornell University, Ithaca, New York 14853-1301, and Departments of Cellular and Molecular Physiology and Pharmacology, Milton S. Hershey Medical Center, Pennsylvania State University College of Medicine, Hershey, Pennsylvania 17033

Received September 20, 2002; Revised Manuscript Received December 17, 2002

ABSTRACT: *S*-Adenosylmethionine decarboxylase (AdoMetDC) is a pyruvoyl-dependent enzyme that catalyzes the formation of the aminopropyl group donor in the biosynthesis of the polyamines spermidine and spermine. The enzyme is synthesized as a protein precursor and is activated by an autocatalytic serinolysis reaction that creates the pyruvoyl group. The autoprocessing reaction proceeds via an N → O acyl rearrangement, generating first an oxyoxazolidine anion intermediate followed by an ester intermediate. A similar strategy is utilized in self-catalyzed protein splicing reactions and in autoproteolytic activation of protein precursors. Mutation of Ser68 to alanine in human AdoMetDC prevents processing by removing the serine side chain necessary for nucleophilic attack at the adjacent carbonyl carbon atom. We have determined the X-ray structure of the S68A mutant and have constructed models of the proenzyme and the oxyoxazolidine intermediate. Formation of the oxyoxazolidine intermediate is promoted by a hydrogen bond from Cys82 and stabilized by a hydrogen bond from Ser229. These observations are consistent with mutagenesis studies, which show that the C82S and C82A mutants process slowly and that the S229A mutant does not process at all. Donation of a proton by His243 to the nitrogen atom of the oxyoxazolidine ring converts the oxyoxazolidine anion to the ester intermediate. The absence of a base to activate the hydroxyl group of Ser68 suggests that strain may play a role in the cleavage reaction. Comparison of AdoMetDC with other self-processing proteins shows no common structural features. Comparison to histidine decarboxylase and aspartate decarboxylase shows that these pyruvoyl-dependent enzymes evolved different catalytic strategies for forming the same cofactor.

Spermine and spermidine are essential growth factors. Their levels are highly regulated primarily by the action of the polyamine biosynthetic enzymes *S*-adenosylmethionine decarboxylase (AdoMetDC)[1] and ornithine decarboxylase and by the polyamine degradative enzyme spermine/spermidine N^1-acetyl transferase. During cell division, the levels of both transcription and translation of AdoMetDC increase (*1*, *2*). AdoMetDC activity is stimulated by putrescine, which also accelerates the processing reaction (*3*, *4*). Putrescine is also a substrate for spermidine synthase, the next enzyme in the polyamine biosynthetic pathway. Ubiquitin-mediated degradation further regulates AdoMetDC activity (*5*−*7*). Because of the critical role of polyamines in cell growth, AdoMetDC and other polyamine biosynthetic enzymes are considered targets for the design of anticancer drugs.

AdoMetDC catalyzes the decarboxylation of *S*-adenosylmethionine, forming decarboxylated *S*-adenosylmethionine (dcAdoMet), the aminopropyl group donor in polyamine biosynthesis (*6*, *8*). The decarboxylation reaction utilizes a covalently attached pyruvoyl cofactor, which is generated by cleavage of the inactive proenzyme. For the human enzyme, the resulting β-chain consists of residues 1−67 and the α-chain consists of residues 68−329 with the pyruvoyl group at its N-terminus.

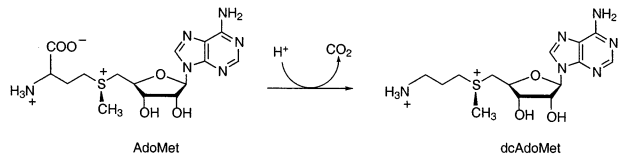

The chemical mechanism of pyruvoyl group formation is well-established (*9*−*11*) (Scheme 1). Serinolysis proceeds by an N → O acyl rearrangement, forming an ester intermediate (*12*, *13*). The ester is resolved by β-elimination, creating dehydroalanine. Tautomerization of dehydroalanine

[†] This work was supported by the Biomedical Research Resource Program (RR-01646) and the National Cancer Institute (Grant CA-18138 to A.E.P.) of the National Institutes of Health. S.E.E. is indebted to the W. M. Keck Foundation and the Lucille P. Markey Charitable Trust.

[‡] The coordinates of the S68A AdoMetDC structure have been deposited in the Protein Data Bank as entry 1MSV.

* To whom correspondence should be addressed: Department of Chemistry and Chemical Biology, Cornell University, Ithaca, NY 14850. Telephone: (607) 255-7961. Fax: (607) 255-1227. E-mail: see3@cornell.edu.

[§] Cornell University.

[||] Pennsylvania State University College of Medicine.

[1] Abbreviations: AdoMetDC, *S*-adenosylmethionine decarboxylase; HisDC, histidine decarboxylase; AspDC, aspartate decarboxylase; PCR, polymerase chain reaction; Tris, tris(hydroxymethyl)aminomethane; PEG, poly(ethylene glycol); HPLC, high-performance liquid chromatography; MGBG, methylglyoxal bis(guanylhydrazone); DTT, dithiothreitol; rms, root-mean-square.

10.1021/bi0268854 CCC: $25.00
Published on Web 02/07/2003

Scheme 1

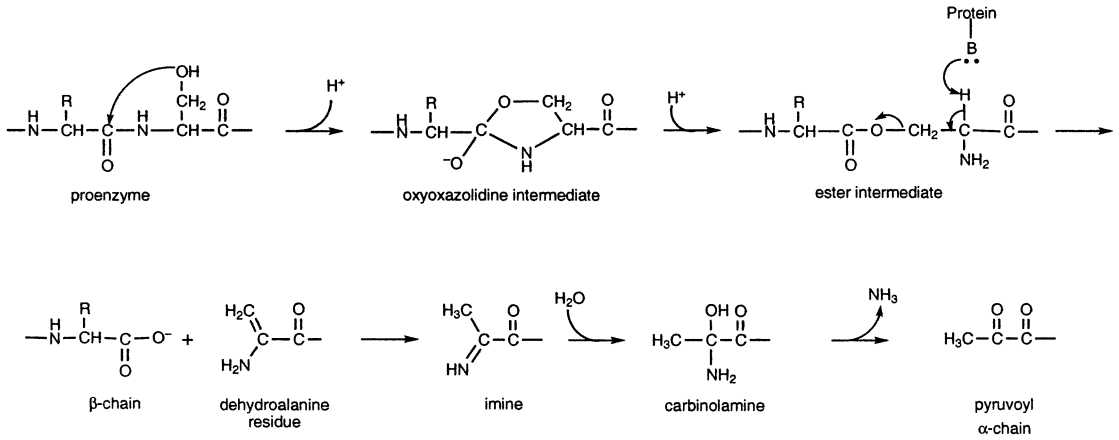

produces an imine, which is converted first to a carbinolamine and then deaminated to form the covalently attached pyruvoyl group. N → O or N → S acyl rearrangements are also involved in protein splicing by inteins (*14*), *hedgehog* autoprocessing (*15*, *16*), and autoproteolysis of glycosylasparaginase (*17*, *18*); however, the mechanism for resolving the ester intermediate varies among these proteins.

The X-ray structures of pyruvoyl-dependent human AdoMetDC (PDB entry 1JEN), *Escherichia coli* aspartate decarboxylase (PDB entry 1AW8), and *Lactobacillus* 30a histidine decarboxylase (PDB entry 1PYA) are known. An ester intermediate has been observed directly in the structures of the H243A mutant of human AdoMetDC (PDB entry 1JL0) and in one monomer of the tetrameric *E. coli* aspartate decarboxylase structure (*9*, *19*). The oxyoxazolidine intermediate has not been directly observed. Attempts to better understand the acyl rearrangement have led to a number of mutant intein and glycosylasparaginase structures that trap the enzymes in a prespliced or precleaved state (*17*, *18*, *20*). The S68A mutant structure of human AdoMetDC reported here traps the enzyme in the proenzyme form by removing the hydroxyl needed for acyl rearrangement and is the first example of a preprocessed pyruvoyl-dependent enzyme structure. The structure allows us to examine the roles of specific amino acids and the role of strain in the mechanism of the processing reaction.

EXPERIMENTAL PROCEDURES

The Chameleon double-stranded site-directed mutagenesis kit was from Stratagene (La Jolla, CA). The Talon metal affinity resin and Ligation Express kit were products of Clontech (Palo Alto, CA). The pQE30 vector was from Qiagen (Valencia, CA). The restriction enzymes were from Gibco BRL (Gaithersburg, MD), Promega, and New England BioLabs (Beverly, MA). Sequenase version 2.0 DNA polymerase was from Amersham (Arlington Heights, IL). Human AdoMetDC cDNA was subcloned into the pGEM3Zf$^-$ vector to form pCM9 (*21*) and into the pQE30 vector to form pHIS-SAM (*22*).

Mutagenesis and Plasmid Construction. The C82A alteration was introduced by site-directed mutagenesis in pCM9 as described previously (*21*). This was used to construct pHIS-hSAMC82A by digestion with *Csp*45I and *Sal*I and insertion of the resulting fragment into pHIS-SAM cut with the same enzymes (*22*).

Enzyme Expression and Purification. AdoMetDC was purified as described previously (*23*). The S68A mutant is in a pQE30 vector, which replaces the N-terminal methionine with MRGS(His)$_6$GS. An overnight culture of the S68A AdoMetDC-expressing XL-1 Blue/JM109 *E. coli* cells was grown in Luria-Bertani (LB) medium with 50 μg/mL ampicillin. Larger cultures of LB medium and 50 μg/mL ampicillin were then inoculated with a 1:100 dilution (v/v) of the overnight culture. Cells were grown at 37 °C until Abs$_{600}$ reached 0.6−0.8, after which 0.3 mM isopropyl thio-β-D-galactoside was added and cells were grown for an additional 5−6 h. Cells were harvested by centrifugation at 5000*g* for 20 min and then frozen and stored. Frozen cell pellets were resuspended in wash buffer [50 mM tris(hydroxymethyl)aminomethane-HCl (Tris) (pH 8.0), 200 mM NaCl, and 2.5 mM putrescine] and lysed by sonication or treatment with a French press. Cellular debris was removed by centrifugation at 20000*g* for 30 min.

The cellular lysate was incubated with Talon metal affinity resin that had been preequilibrated with wash buffer for 30 min. The resin was poured into a column and washed until the Abs$_{280}$ reached the baseline, typically 5−10 column volumes. The column was then washed with 5−10 column volumes of 50 mM Tris-HCl (pH 8.0), 395 mM NaCl, 2.5 mM putrescine, and 5 mM imidazole. The enzyme was eluted with 50 mM Tris-HCl (pH 8.0), 200 mM imidazole, 200 mM NaCl, and 2.5 mM putrescine and then dialyzed into 10 mM Tris-HCl (pH 7.5), 200 mM NaCl, and 5 mM dithiothreitol (DTT). The enzyme was concentrated to 5 mg/mL, frozen, and stored at −80 °C.

Crystallization. The purified enzyme was thawed on ice and further concentrated to 10 mg/mL with Amicon microcon centrifugal concentrators. Crystals were grown by the hanging drop method in 14−16% polyethylene glycol (PEG) 8000 (w/w), 100 mM Tris-HCl (pH 8.0), and 10 mM DTT at 4 °C. Crystals grew overnight, but deteriorated if kept longer than 2−3 weeks. Crystals were flash-frozen in liquid nitrogen after a sequential transfer into 2, 5, 8, 10, 15, and finally 18% glycerol, 17% PEG 8000 (w/w), 25 mM Tris-HCl (pH 8.0), and 200 mM NaCl with approximately 2 min between transfers. Crystals belong to space group $P2_1$ with two monomers per asymmetric unit (a = 73.94 Å, b = 56.38 Å, c = 99.19 Å, and β = 110.97°).

Data Collection and Processing. Data were collected at Cornell High Energy Synchrotron Source beam line A-1 at

Table 1: Data Collection and Refinement Statistics for the S68A AdoMetDC Model[a]

Data Collection Statistics		
	99−1.70 Å resolution	1.79−1.70 Å resolution
no. of reflections	551036	41351
no. of unique reflections	82984	11752
redundancy	6.6	3.5
completeness (%)	98.7	96.3
R_{sym} (%)	11.7	28.0
I/σ	3.9	1.8

Refinement Statistics	
resolution (Å)	99−1.75 (1.76−1.75)
R_{factor}	0.210 (0.279)
R_{free}	0.238 (0.320)
no. of non-H atoms	
protein	5157
ligand	28
water	306
B-factor (Å^2)	
protein	27.6
Tris	27.4
putrescine	20.3
water	31.3
rms deviation	
bonds (Å)	0.006
angles (deg)	1.25
dihedrals (deg)	25.0

[a] The numbers in parentheses represent statistics for the highest-resolution bin.

0.930 Å on an Area Detector Systems Corp. Quantum 4 X-ray detector. Two 180° passes were made on one crystal with exposure times of 30 and 2 s. A single 180° pass with 20 s exposures was made on a second crystal. The data were indexed using DPS (*24*, *25*) and integrated and scaled with MOSFLM and SCALA from the CCP4 suite (*26*). Resolution ranges for each data set were chosen to minimize poorly measured data and maximize redundancy in the final merged data set. Data were integrated to 1.7 Å, although only reflections to 1.75 Å were included in the refinement (Table 1).

Structure Determination and Refinement. CNS version 1.0 (*27*) was used for molecular replacement with a search model consisting of the methylglyoxal bis(guanylhydrazone) complex structure (PDB entry 1I76) minus water molecules and seven residues in the sequence before and after the site of pyruvate formation. CNS was also used for model refinement and automated water addition (*28*, *29*). Model building was done with the program O (*30*). Density for the missing residues was located in composite simulated annealing omit maps. A test set consisting of 10% of the measured reflections was set aside for monitoring the free *R* value (*31*). Parameter and topology files for ligands were defined from models built into density using modified Engh and Huber (*32*) parameters.

A bound putrescine molecule was identified in each subunit at positions consistent with previous AdoMetDC structures (*19*, *33*). A Tris molecule was identified and modeled at the entrance to the active site. Alternate conformations were added for 35 residues. Model refinement and quality were assessed periodically by monitoring R_{factor} and R_{free}, which converged to 21.0 and 23.8%, respectively. The final model contains 639 residues, two putrescine molecules, two Tris molecules, and 306 water molecules. Refinement statistics are reported in Table 1.

Molecular Modeling. Computational models were constructed using the OPLS-AA force field (*34*), the GB/SA solvation model (*35*), and the TNCG minimizer (*36*) as implemented in version 7.2 of the program MacroModel (*37*). Hydrogen atoms were added to the S68A crystal structure; water molecules were removed, and the resulting structure was energy minimized. A base shell of atoms was defined to include any residue having at least one atom within 14 Å of residues 65−69. An extended shell of atoms included all atoms within two bonds of the base shell. This extended shell was used as the starting point for the models of the proenzyme and the oxyoxazolidine intermediate.

The S68 model was generated by mutating Ala68 to serine and performing 140 000 steps of conformational searching using the MCMM (*38*) and simple l-LMOD (*39*) methods to generate trial structures. Residues 65−69 and the side chains of residues 7, 82, 221, 223, 229, and 243 were allowed to move freely, while all other atoms were locked in place.

The oxyoxazolidine model was created by attaching the side chain oxygen atom of Ser68 to the carbonyl carbon of Glu67, rotating the Ser229 side chain, and manually positioning the exocyclic oxygen atom within good hydrogen bonding distance of the Ser229 side chain. The exocyclic oxygen atom was locked in place, and the structure was energy minimized to allow the rest of the structure to adjust. The restraint on the exocyclic oxygen was then removed, and the structure was reminimized. This structure was used to initiate limited MCMM/*l*-LMOD conformational searching. Maintaining a good hydrogen bonding distance between Ser229 and the exocyclic oxygen required additional flexibility in the model, obtained by adding residues 52, 63, 64, 228, and 230, and the backbone atoms of residues 221 and 229, to the list of unrestrained atoms. One explicit water molecule, also unrestrained, was included between the carbonyl groups of residues 66 and 68.

The model of the ester intermediate with His243 was generated from the H243A crystal structure by mutating residue Ala243 to histidine. Hydrogen atoms were added; all water molecules except the one between the carbonyl groups of residues 66 and 68 were removed, and the resulting structure was energy minimized with all atoms unrestrained.

For all three models, structures were minimized to a gradient of less than 0.05 kJ mol^{-1} Å^{-1} with van der Waals cutoffs of at least 8 Å and electrostatic cutoffs of at least 20 Å.

RESULTS

Structure of S68A AdoMetDC. The overall structure of the S68A mutant (Figure 1) is similar to the structures of the H243A mutant AdoMetDC (*19*) and the fully processed wild-type AdoMetDC (*23*, *33*) with a few important exceptions. In contrast to the ester linkage observed for the H243A mutant and the pyruvoyl group observed for the processed enzyme, the electron density for the S68A mutant clearly shows a peptide bond between residues Glu67 and Ser68 (Figure 2). Residues 65−68 form a β-turn that connects the ends of two adjacent antiparallel β-strands, β3 and β4. In the S68A structure, the β-turn most closely resembles a type II β-turn, while in the H243A structure, it is closest to a type I β-turn.

Binding Sites for Putrescine and Tris. One putrescine molecule and one Tris molecule are bound to each AdoMet-

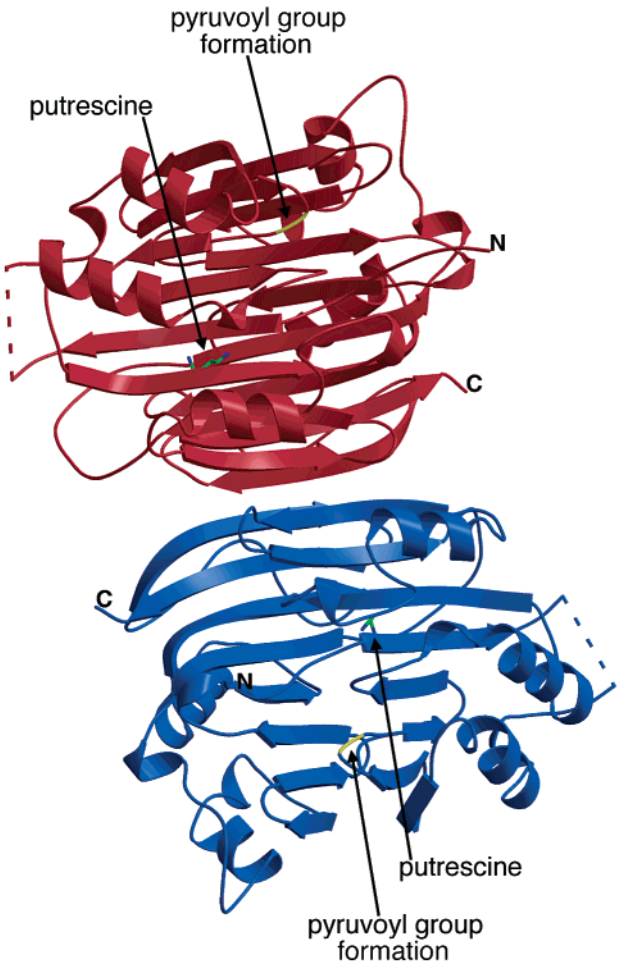

FIGURE 1: Dimer of S68A AdoMetDC showing the sites of pyruvoyl group formation and putrescine binding. Each protomer consists of a four-layer αββα sandwich, in which the two β-sheets are interconnected by a single loop. By convention, the first 67 residues in the monomer are termed the β-chain and the remaining residues the α-chain. After serinolysis of the proenzyme, the pyruvoyl group is formed on the N-terminus of the α-chain. The dashed lines represent loops that were missing in the electron density. This figure was generated with BOBSCRIPT (*51*, *52*) and Raster3D (*53*).

DC protomer. The putrescine binding site is similar to that observed for the wild-type (*33*) and H243A mutant AdoMetDCs (*19*). The average *B*-factor for the putrescine atoms is 20.3 Å^2, lower than the average value of 27.6 Å^2 for all protein atoms. One putrescine amino group donates hydrogen bonds to the side chains of Glu15, Asp174, and Thr176. The other amino group forms hydrogen bonds with three water molecules, which in turn hydrogen bond to Ser113, Glu178, and Glu256.

The Tris binding sites in S68A, H243A, and wild-type AdoMetDC (*19*) are similar but also exhibit important differences (Figure 3). For both the S68A and H243A structures, the Tris molecule forms hydrogen bonds with the carboxylate of Glu247 and the backbone carbonyl oxygen of Cys226. The Tris molecule is sandwiched between the phenyl groups of Phe7 and Phe223 in both structures and is reminiscent of the interactions of these two residues with substrate analogues and inhibitors observed in the AdoMetDC complex structures (*33*). Unlike the Tris molecule in the H243A structure, which forms a number of hydrogen bonds

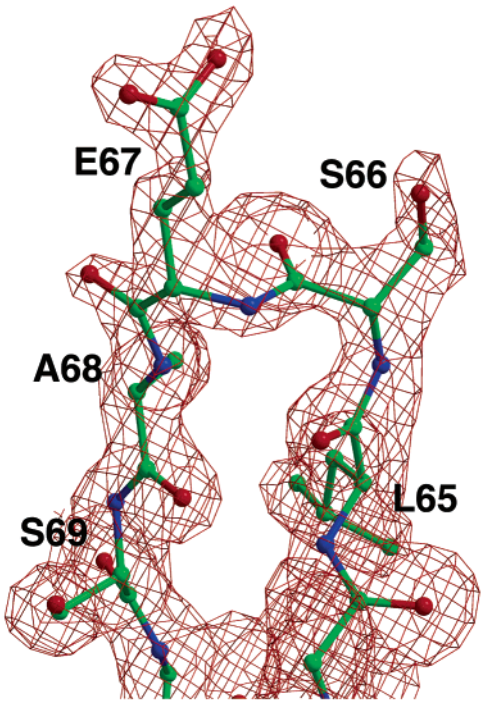

FIGURE 2: Electron density for the type II β-turn of residues 65−68 in S68A mutant AdoMetDC. The electron density was calculated using phases from a model for which residues 65−68 were removed. The model corresponds to the final refined S68A structure. This figure was generated with BOBSCRIPT (*51*, *52*) and Raster3D (*53*).

with ordered water molecules, the Tris molecule in the S68A structure forms two additional hydrogen bonds with the carboxylate of Glu67. The difference in Tris binding is due mainly to a change in loop conformation that occurs upon formation of the ester, suggesting that Tris might inhibit the processing reaction. The average *B*-factor for the Tris molecule is 27.4 Å^2.

Residues Near the Glu67-Ala68 Cleavage Site in S68A. The S68A mutation of AdoMetDC traps the enzyme in the proenzyme form by removing the hydroxyl needed for the N → O acyl rearrangement. Nevertheless, many of the interactions that promote the N → O acyl rearrangement leading to generation of the pyruvoyl group are present. These involve the sulfhydryl of Cys82, which is 3.1 Å from the carbonyl of Glu67, and the hydroxyl oxygen atom of Ser229, which is 4.9 Å from the carbonyl of Glu67 (Figure 4A). One water molecule ($W_{C'}$) that interacts with Ser229 is in a position similar to that of a water molecule in the H243A mutant structure and is one of three water molecules arranged tetrahedrally around the amino group in the ester (*19*).

Model of the AdoMetDC Proenzyme. Computational modeling of the proenzyme showed a collection of structures of which approximately 45% have Ser68 positioned to attack the carbonyl carbon atom of Glu67 (Figure 4A). In these structures, the Ser68 hydroxyl group is positioned to donate a hydrogen bond to the carbonyl group of either Ser66 or Glu67, and the closest contact between the Glu67 carbonyl oxygen atom and Ser229 is 3.9 Å. Nearly all (95%) of the lowest-energy structures showed a type II β-turn for residues 65−68 with Ser68 in the fourth position. The side chain of Glu67 showed the greatest variation.

Model of the Oxyoxazolidine Intermediate. Formation of the five-membered oxyoxazolidine ring adds additional

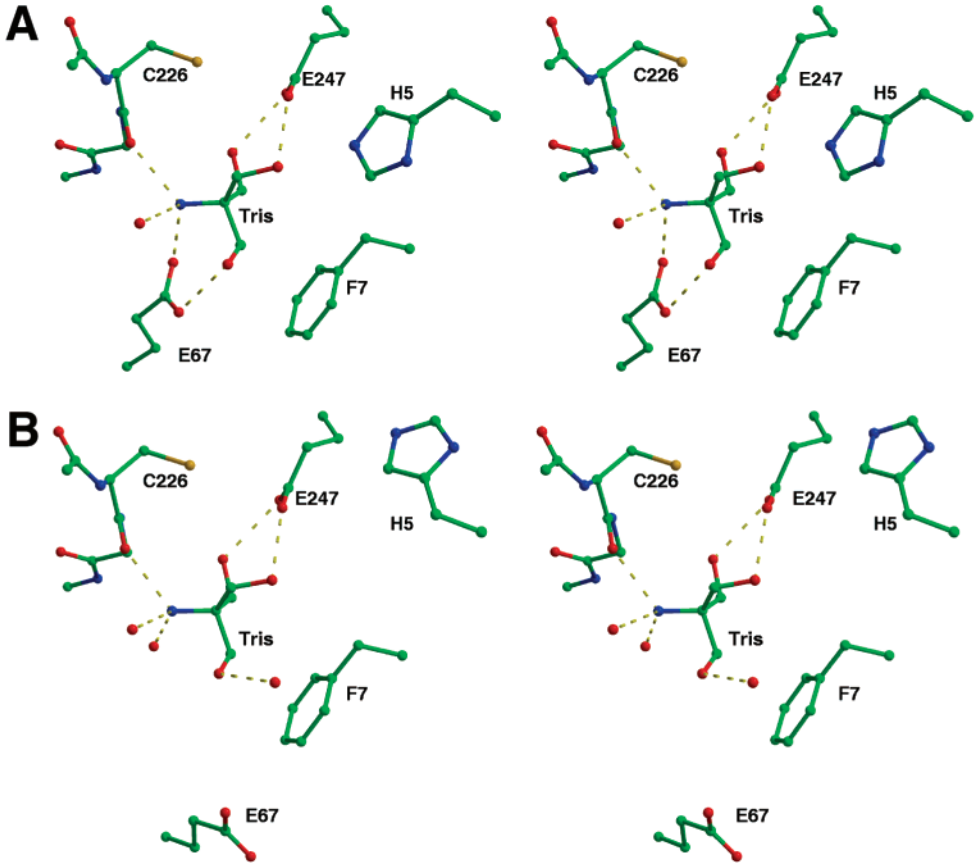

FIGURE 3: Tris binding sites in human AdoMetDC. (A) S68A mutant AdoMetDC. (B) H243A mutant AdoMetDC. In the S68A mutant structure, additional hydrogen bonds are formed with Glu67. This figure was generated with BOBSCRIPT (*51*, *52*) and Raster3D (*53*).

constraints to the turn of residues 65−68. Some higher-energy structures showed hydrogen bonds between Ser229 and the exocyclic oxygen of the oxyoxazolidine ring. Some low-energy structures showed Ser229 donating a hydrogen bond to the conserved water molecule and the exocyclic oxygen accepting hydrogen bonds from the Cys82 side chain and amide. In contrast to the proenzyme model, the oxyoxazolidine models exhibited both type I and type II turns.

DISCUSSION

Mechanism of Pyruvoyl Group Formation in Human AdoMetDC. The self-processing reaction of pyruvoyl-dependent enzymes is initiated through an internal serinolysis in which the serine hydroxyl group performs nucleophilic attack at the carbonyl carbon atom of the preceding residue, resulting in an oxyoxazolidine intermediate (*13*). Following rearrangement to the ester, a β-elimination results in dehydroalanine, which undergoes hydrolysis to form the pyruvoyl group and release ammonia (Scheme 1).

The S68A mutant does not process because it lacks the serine hydroxyl group; in contrast, the S68C and S68T mutants are processed slowly, giving a thiocarboxylate at position 67 (2% of the wild type) and an α-ketobutyrate (4% of the wild type) at position 68, respectively (*40*). The AdoMetDC proenzyme was modeled by adding the hydroxyl group to Ala68 in the mutant structure and searching for structures with the lowest energies. In both the S68A mutant and proenzyme model, Ser68 is in the fourth position of a β-turn that most closely resembles a type II turn. In this conformation, the serine hydroxyl oxygen atom can be positioned perpendicular to the plane of the carbonyl group of Glu67 approximately 3 Å from the carbonyl carbon atom (Figure 4A).

Nucleophilic attack by the alcohol on the amide would be assisted by deprotonation of Ser68 and protonation of the carbonyl oxygen atom of Glu67. Examination of the proenzyme model showed several low-energy structures with a hydrogen bond between the Ser68 side chain and the carbonyl oxygen atom of Ser66, but no stronger base was identified near the S68A hydroxyl group, suggesting that this group is not activated by base catalysis. This is not without precedent: *endo*-2-carboxamide-6-hydroxynorbornane undergoes rapid intramolecular ring closure to form the lactone under neutral-pH conditions (*41*, *42*). The side chain of Cys82 was consistently in a position to donate a hydrogen bond to the carbonyl oxygen atom of Glu67, suggesting that this interaction is important for processing. The C82A (*43*) and C82S (unpublished observations) mutants process ~10 times slower. In addition, in the S68A structure, the oxygen atom of Ser229 is approximately 5 Å from the carbonyl group of Glu67; however, several low-energy proenzyme model structures showed Ser229 is close enough to donate a hydrogen bond.

In the oxyoxazolidine intermediate, the hydroxide oxygen atom moves ~1 Å closer to Ser229, and after conformational searching had been carried out, several higher-energy structures showed a good hydrogen bond to Ser229 (Figure 4B). This model is consistent with site-directed mutagenesis data, which show that the S229A mutant does not process at all whereas the mutant S229T processes readily (85% of

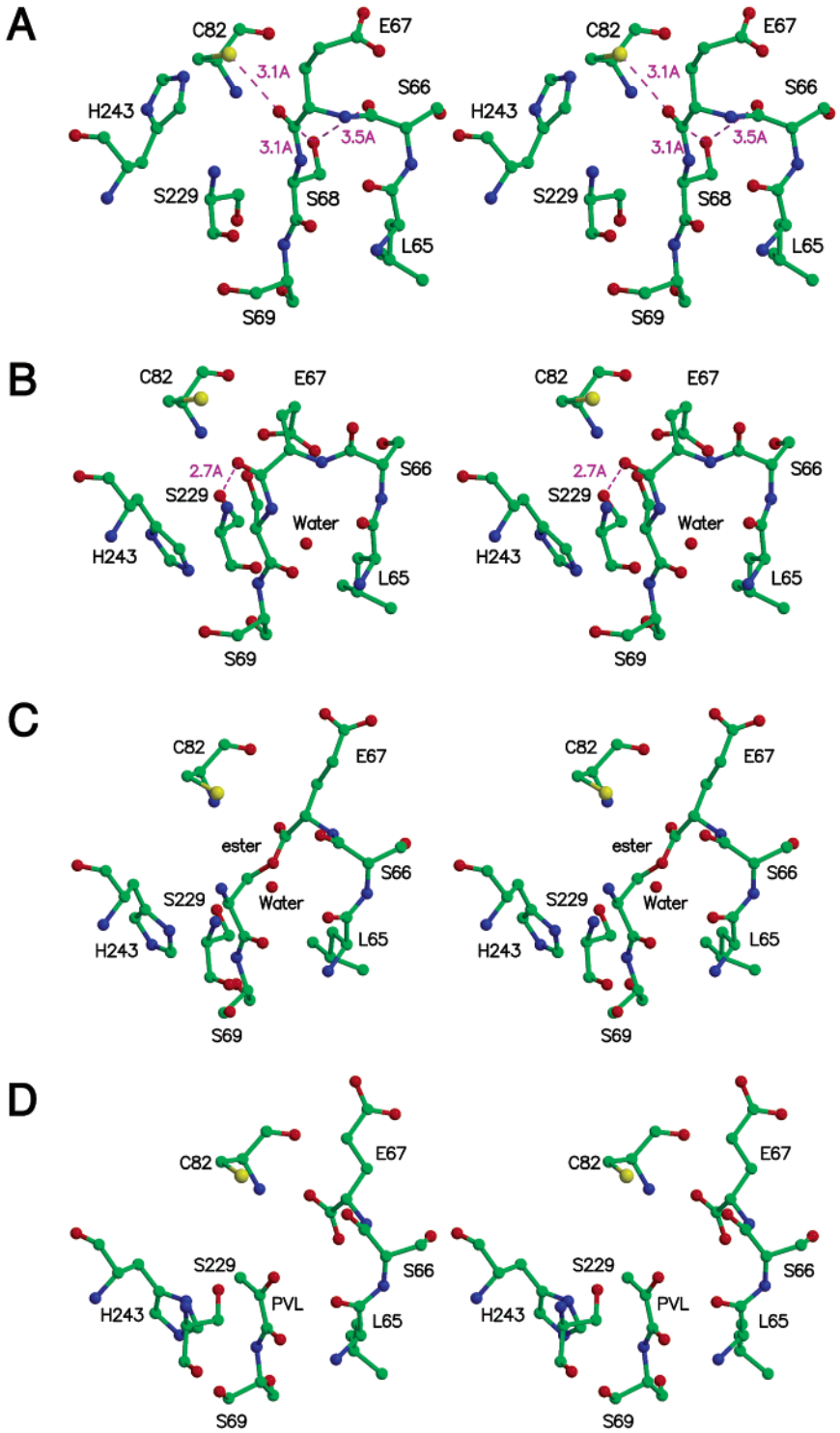

FIGURE 4: Stereodiagrams illustrating consecutive steps in the processing of the AdoMetDC proenzyme. (A) Computer model of the wild-type enzyme, generated from the S68A crystal structure by converting Ala68 to serine and performing 140 000 steps of conformational searching. The low-energy conformation shown here places key atoms as required for processing to begin. (B) Oxyoxazolidine intermediate computer model generated from the S68A crystal structure by modifying residue 68 and performing energy minimizations and limited conformational searching. The fully minimized conformation that is shown is a geometrically plausible arrangement of the atoms after attack by the Ser68 hydroxyl from the position shown in panel A, but has more energy than other possible conformations of this structure. (C) Ester intermediate computer model, generated from the H243A crystal structure (*19*) by replacing Ala243 with histidine and performing energy minimization. (D) Crystal structure of the fully processed wild-type enzyme (*23*). Magenta dashed lines show key interactions. PVL is the pyruvoyl group. This figure was created with Molscript (*54*) and Raster3D (*53*).

the wild type) (*4*). The models of the proenzyme and the oxyoxazolidine intermediate structures suggest that Cys82 may initially facilitate the nucleophilic attack and that after the oxyoxazolidine ring forms the Cys82 hydrogen bond is replaced with the Ser229 hydrogen bond. This hydrogen bond is part of a network involving Ser68, the Leu65−Ser66 peptide bond, and a highly conserved water molecule (Figure 5). The Ser229 hydrogen bond to the oxyoxazolidine may also be strengthened by a hydrogen bond from His243 to the Ser229 hydroxyl group.

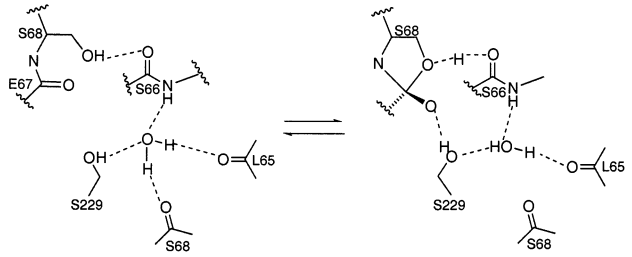

FIGURE 5: Hydrogen bonding for the cleavage site of the AdoMetDC proenzyme and the oxyoxazolidine intermediate.

The model structures show that His243, which could be repositioned to donate a proton to the nitrogen atom of the oxyoxazolidine ring, probably assists the rearrangement of the oxyoxazolidine anion to the ester (Figure 4C). Mechanistic details for the conversion of the ester to the pyruvoyl group (Figure 4D) have been described on the basis of the structure of the H243A AdoMetDC mutant (*4*, *19*). In the H243A mutant, it is possible that a water molecule provides the proton necessary for the ring opening of the oxyoxazolidine intermediate.

Conformational Changes during Processing. The ester intermediate has been directly observed in the structure of the H243A mutant (*19*). The oxyoxazolidine intermediate has been modeled using the S68A structure. Comparison of the structures of the proenzyme, the oxyoxazolidine intermediate, the ester intermediate, and the processed enzyme shows that most of the changes occur at the site of pyruvoyl group formation (Ser68) and in nearby residues Leu65, Ser66, Glu67, Cys82, Ser229, and His243 (Figure 6). For these seven residues, the rms difference in main chain atoms is 0.9 Å for the conversion of the proenzyme to the oxyoxazolidine intermediate, 1.5 Å for the conversion of the oxyoxazolidine intermediate to the ester intermediate, and 0.6 Å for the conversion of the ester intermediate to the active enzyme. The corresponding rms differences in side chain atoms are 3.2, 2.1, and 1.1 Å, respectively. The remainder of the enzyme, including the two antiparallel β-strands (β3 and β4) that are joined by residues 65−68, shows very little change.

Glu67 shows the greatest movement of any residue; however, site-directed mutagenesis shows that Glu67 is not important for processing (*21*). His243 shows significant rotations about both the χ_1 and χ_2 torsion angles during formation of the oxyoxazolidine ring and remains approximately in the rotated position in the structures of the ester intermediate and the processed enzyme. His243 is also likely to be important for the decarboxylation reaction (*19*); however, because the His243 mutant is trapped as the ester intermediate, it is difficult to test this hypothesis experimentally. The conformational flexibility of His243 is consistent with its multiple roles in the autoprocessing and decarboxylation reactions. The side chain of Ser229 in the proenzyme rotates ~100° to form a hydrogen bond and stabilize the oxyoxazolidine anion. The conformations of Ser229 are similar in the two intermediates and the processed enzyme. Leu65, Ser66, and Cys82 exhibit the smallest rms differences of the seven residues, although there is some variation in χ_1 torsion angles for these three residues.

In the proenzyme and oxyoxazolidine intermediate structures, the β-turn most closely resembles a type II β-turn, while in the ester intermediate structure, the β-turn is closest to type I, suggesting that the Ser66−Glu67 peptide rotates during the conversion of the oxyoxazolidine intermediate to the ester intermediate. This conformational change is facilitated by the introduction of the ester bond in place of the peptide bond between residues 67 and 68, which shifts the position of Glu67 and adds an additional atom in the β-turn. In the processed wild-type AdoMetDC, cleavage occurs between the third and fourth positions of the β-turn; however, the remaining main chain torsion angles resemble a type I turn. Conversion of type II to type I β-turns is thought to be a dynamic event in protein structures and has been characterized in homologous crystal structures (*44*). The interconversion can be modeled by a flip of the central peptide unit with an estimated activation energy of 3 kcal/mol (*44*). The loop containing Ser68 in the proenzyme differs significantly from the canonical type II β-turn, having deviations in torsion angles as large as 40°. Therefore, it is possible that conversion from a type II turn in the proenzyme to a type I turn in the ester intermediate facilitates the N → O acyl rearrangement in human AdoMetDC.

Putrescine Activation of Autoprocessing. The rate of autoprocessing is increased by ~1 order of magnitude in the presence of putrescine (*3*, *43*). The structure of AdoMetDC showed that the putrescine binding site is located between the two β-sheets of the monomer and is linked to the active site through a hydrogen bond network involving Lys80, Glu11, and His243 (*19*). The structure suggested that the effect of putrescine could be transmitted to the active site by conformational changes that position key residues or through charge relay or both. The proenzyme and oxyoxazolidine intermediate structures show that neither Glu11 nor Lys80 directly interacts with either Cys82 or Ser229, the residues that affect the first steps of autoprocessing. Glu11 forms a hydrogen bond to a conserved water molecule; however, the water molecule is ~5 Å from Cys82, and a conformational change would be required for formation of a hydrogen bond. His243 is thought to be the proton donor for ring opening to form the ester as well as the proton acceptor in the β-elimination step. Therefore, it is likely that the main factor in putrescine activation is its effect on His243.

Comparison to HisDC and AspDC. AdoMetDC represents a novel structural fold that is different from the other structurally characterized pyruvoyl-dependent enzymes *E. coli* aspartate decarboxylase (*9*) and *Lactobacillus* 30a histidine decarboxylase (*45*, *46*). Although the ester intermediate has been observed in the H243A mutant of AdoMetDC and in the disordered structure of AspDC (*9*), S68A AdoMetDC is the first example of the proenzyme structure of a pyruvoyl-dependent enzyme. In human AdoMetDC, the site of pyruvoyl formation occurs in a type II β-turn that joins adjacent β-strands β3 and β4 within the same β-sheet (Figure 7A).

In HisDC, the site of pyruvoyl formation is between a β-strand (residues 74−80, β4) of β-sheet II and a short β-strand (residues 82−84, β5) of β-sheet III; these two strands do not directly interact (Figure 7B). In HisDC, Ser82 provides the oxygen atom for ester formation and the adjacent residue, Ser81, also plays a role in processing. The S81A HisDC does not process to form a pyruvoyl group at position 82. Instead, slow cleavage occurs at the adjacent peptide bond (residues 80 and 81), resulting in a new C-terminus at

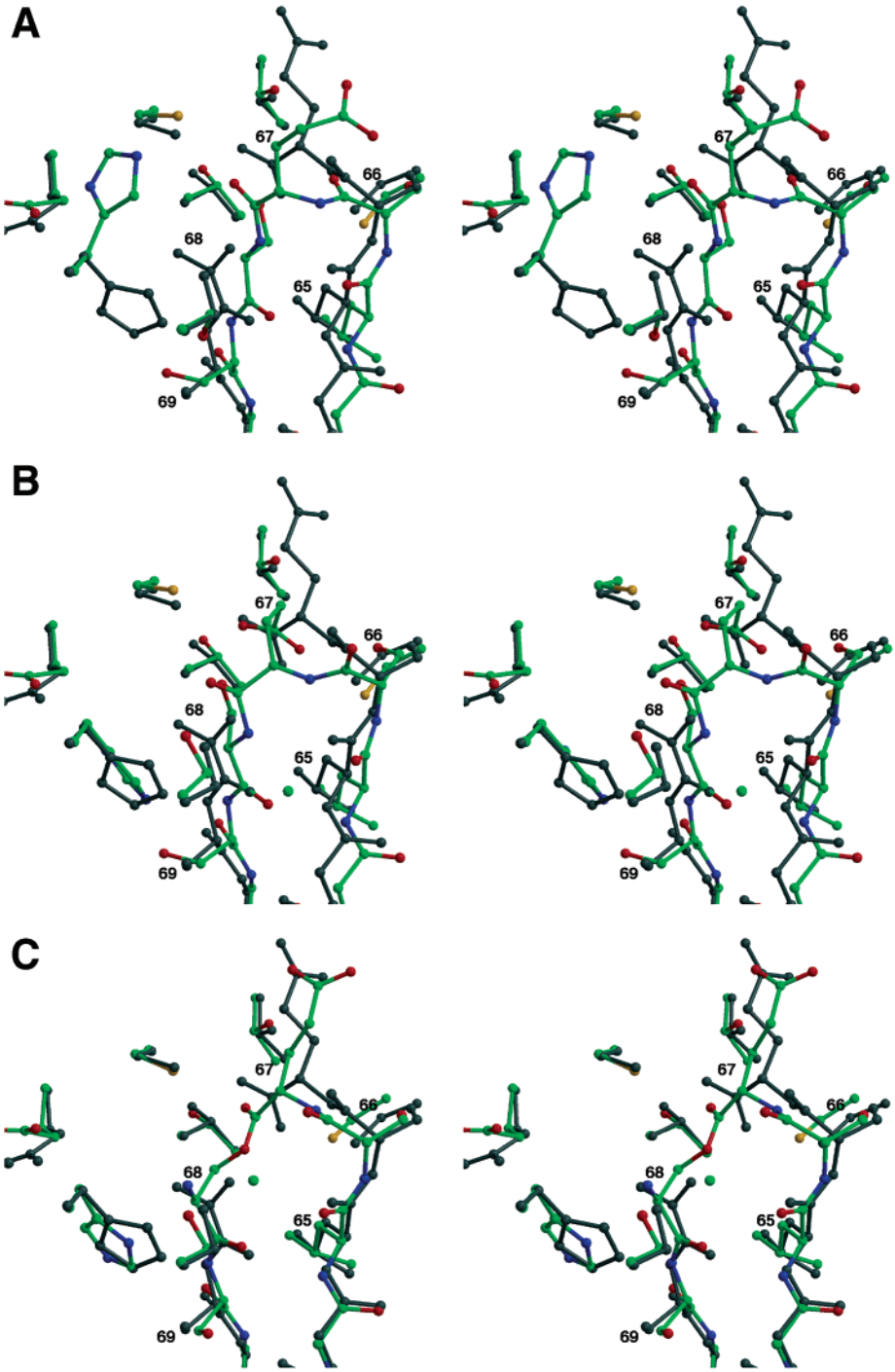

FIGURE 6: Stereoviews showing the conformational changes during AdoMetDC processing. The three panels show structures for the various steps of processing with green bonds compared to the structure of the processed wild-type enzyme with blue bonds. (A) Proenzyme based on the S68A mutant. (B) Oxyoxazolidine anion intermediate generated by computer modeling. (C) Ester intermediate based on the H243A mutant. This figure was generated with BOBSCRIPT (*51*, *52*) and Raster3D (*53*).

position 80 and a new N-terminus at position 81 (*45*). This observation led to the proposal that conformational strain plays an important role in pyruvoyl formation for wild-type HisDC and in the incorrect self-cleavage reaction of S81A HisDC. The absence of precursor structures prevents a more detailed analysis of the HisDC processing mechanism.

In AspDC, the site of pyruvoyl group formation is located in a five-membered loop between strand $\beta1'$ and strand $\beta2$ (Figure 7C). These two strands are part of the same β-sheet but are separated by an additional strand ($\beta5$). It was hypothesized that because the loop was shorter than other loops with the same topology, strain might play a role in autoprocessing (*9*). Unlike dimeric AdoMetDC and hexameric HisDC, for which pyruvoyl group formation does not involve subunit−subunit interactions, tetrameric AspDC displays negative cooperativity, resulting in a major species with three processed subunits and one unprocessed subunit. For AspDC, it was proposed that Ser25 could be activated through a hydrogen bonding network involving Tyr58 of one subunit and Lys9 and His11 of an adjacent subunit and that Tyr58 could be the proton donor for the conversion of the oxyoxazolidine intermediate to the primary amine (*9*).

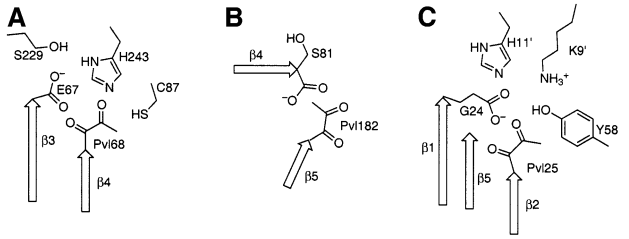

FIGURE 7: Sites of pyruvoyl group formation: (A) AdoMetDC, (B) HisDC, and (C) AspDC. Arrows represent β-strands. Key residues are shown; residue numbers with primes are from an adjacent protomer.

Comparison to Other Autoprocessing Proteins. Pyruvate formation is similar in mechanism to other protein processing reactions such as autoproteolytic activation of enzyme precursors and intein self-cleavage reactions. In *Flavobacterium* glycosylasparaginase, the hydroxyl of Thr152 hydrogen bonds with one of the carboxylate oxygen atoms of Asp151 (*47*). This interaction is believed to enhance the nucleophilicity of the hydroxyl group. Thr152 is also oriented toward the scissile peptide bond, which is in a strained (ω < 160°) *trans* conformation. In the GyrA intein from *Mycobacterium xenopi*, the scissile peptide bond is in a *cis* conformation (*20*). The nucleophilicity of the sulfhydryl group is enhanced by a hydrogen bond to Ser53. The cysteine to serine mutation does not process, possibly because of the higher pK_a of the hydroxyl group. The oxythiazolidine intermediate is stabilized by hydrogen bonds to the hydroxyl of Thr72 and Nδ of Asn74 (*20*). His75 serves as the proton donor for the breakdown of the tetrahedral oxythiazolidine. The crystal structure of the PI-SceI miniprecursor from *Saccharomyces cerevisiae* (*48*) supports many of the conclusions resulting from the GyrA intein structure. His79 (analogous to His75 in the GyrA structure) is in a position to protonate the tetrahedral intermediate and form the thioester. The oxythiazolidine intermediate is stabilized by hydrogen bonds from Nδ of Asn76 and Oγ of Thr78. Unlike the GyrA structure, the scissile peptide bond is in a *trans* conformation and the closest residue that could polarize the sulfhydryl group prior to nucleophilic attack is Asn76. The only evidence of conformational strain is an N$-C_\alpha-$C angle of 100°.

The peptide bonds in the turn of residues 65−68 of the S68A AdoMetDC crystal structure are in a standard *trans* conformation. This differs from glycosylasparaginase and the PI-SceI intein, both of which have distorted *trans* conformations at the scissile peptide position (*18*, *49*, *50*), and the GyrA intein, which has a *cis* conformation at the scissile peptide position (*20*). This suggests that strain plays a less important role in the processing of the AdoMetDC proenzyme; however, some evidence of strain is seen in the torsion angles of the type II β-turn of the proenzyme model structures, which deviate from their standard values by as much as 40°.

CONCLUSIONS

Several factors could potentially aid the formation of the ester intermediate in reactions that involve N → O or N → S acyl rearrangements. These include (1) geometrical constraints that position the nucleophilic side chain for attack at the adjacent carbonyl carbon atom, (2) activation of the nucleophile with a base or hydrogen bond acceptor, (3) stabilization of the oxyoxazolidine (or oxythiazolidine) anion by a proton donor or hydrogen bond donor, (4) conformational strain in the scissile bond, and (5) protonation of the amino group during ester formation. Comparison of the structures of proteins that utilize N → O or N → S acyl rearrangements in autoprocessing suggests that all of these factors play a role but vary in their importance for different reactions. In human AdoMetDC, no single factor appears to be primarily responsible for autoprocessing. Understanding the mechanism of pyruvoyl group formation may be useful in the design of novel compounds that inhibit AdoMetDC activity by preventing the processing of the proenzyme.

ACKNOWLEDGMENT

We thank Prof. Tadhg Begley for thoughtful discussions and Ms. Leslie Kinsland for her assistance in the preparation of the manuscript. We thank the Cornell High Energy Synchrotron Source for providing beam time.

REFERENCES

1. Hardin, M. S., and Hurta, R. A. R. (2002) *J. Cell. Biochem. 84* (Suppl.), 349−358.
2. Hurta, R. A. R. (2001) *J. Cell. Biochem. 36* (Suppl.), 209−221.
3. Stanley, B. A., Shantz, L. M., and Pegg, A. E. (1994) *J. Biol. Chem. 269*, 7901−7907.
4. Xiong, H., and Pegg, A. E. (1999) *J. Biol. Chem. 274*, 35059−35066.
5. Pegg, A. E., Xiong, H., Feith, D., and Shantz, L. M. (1998) *Biochem. Soc. Trans. 26*, 580−586.
6. Stanley, B. A. (1995) in *Polyamines: Regulation and Molecular Interaction* (Casero, R. A., Jr., Ed.) R. G. Landes Co., Austin, TX.
7. Svensson, F., Mett, H., and Persson, L. (1997) *Biochem. J. 322*, 297−302.
8. Pegg, A. E. (1986) *Biochem. J. 234*, 249−262.
9. Albert, A., Dhanaraj, V., Genschel, U., Khan, G., Ramjee, M. K., Pulido, R., Sibanda, B. L., von Delft, F., Witty, M., Blundell, T. L., Smith, A. G., and Abell, C. (1998) *Nat. Struct. Biol. 5*, 289−293.
10. Gallagher, T., Rozwarski, D. A., Ernst, S. R., and Hackert, M. L. (1993) *J. Mol. Biol. 230*, 516−528.
11. Parks, E. H., Ernst, S. R., Hamlin, R., Xuong, N. H., and Hackert, M. L. (1985) *J. Mol. Biol. 182*, 455−465.
12. Recsei, P. A., and Snell, E. E. (1984) *Annu. Rev. Biochem. 53*, 357−387.
13. van Poelje, P. D., and Snell, E. E. (1990) *Annu. Rev. Biochem. 59*, 29−59.
14. Paulus, H. (1998) *Chem. Soc. Rev. 27*, 375−386.
15. Porter, J. A., Young, K. E., and Beachy, P. A. (1996) *Science 274*, 255−259.
16. Hall, T. M., Porter, J. A., Young, K. E., Koonin, E. V., Beachy, P. A., and Leahy, D. J. (1997) *Cell 91*, 85−97.
17. Guan, C., Cui, T., Rao, V., Liao, W., Benner, J., Lin, C. L., and Comb, D. (1996) *J. Biol. Chem. 271*, 1732−1737.
18. Xu, Q., Buckley, D., Guan, C., and Guo, H. C. (1999) *Cell 98*, 651−661.
19. Ekstrom, J. L., Tolbert, W. D., Xiong, H., Pegg, A. E., and Ealick, S. E. (2001) *Biochemistry 40*, 9495−9504.
20. Klabunde, T., Sharma, S., Telenti, A., Jacobs, W. R., Jr., and Sacchettini, J. C. (1998) *Nat. Struct. Biol. 5*, 31−36.
21. Stanley, B. A., Pegg, A. E., and Holm, I. (1989) *J. Biol. Chem. 264*, 21073−21079.
22. Xiong, H., Stanley, B. A., and Pegg, A. E. (1999) *Biochemistry 38*, 2462−2470.
23. Ekstrom, J. E., Matthews, I. I., Stanley, B. A., Pegg, A. E., and Ealick, S. E. (1999) *Structure 7*, 583−595.
24. Powell, H. R. (1999) *Acta Crystallogr. D55*, 1690−1695.
25. Steller, I., Bolotovosky, R., and Rossman, M. G. (1997) *J. Appl. Crystallogr. 30*, 1036−1040.
26. Collaborative Computational Project Number 4 (1994) *Acta Crystallogr. D50*, 760−763.

27. Brünger, A. T., Adams, P. D., Clore, G. M., DeLano, W. L., Gros, P., Grosse-Kunstleve, R. W., Jiang, J. S., Kuszewski, J., Nilges, M., Pannu, N. S., Read, R. J., Rice, L. M., Simonson, T., and Warren, G. L. (1998) *Acta Crystallogr. D54*, 905−921.
28. Kleywegt, G. J., and Brunger, A. T. (1996) *Structure 4*, 897−904.
29. Read, R. J. (1986) *Acta Crystallogr. A42*, 140−149.
30. Jones, T. A., Zou, J.-Y., Cowan, S. W., and Kjeldgaard, M. (1991) *Acta Crystallogr. A47*, 110−119.
31. Brünger, A. T. (1992) *Nature 355*, 472−475.
32. Engh, R. A., and Huber, R. (1991) *Acta Crystallogr. A47*, 392−400.
33. Tolbert, D. W., Ekstrom, J. L., Mathews, I. I., Secrist, J. A. I., Kapoor, P., Pegg, A. E., and Ealick, S. E. (2001) *Biochemistry 40*, 9484−9494.
34. Jorgenson, W. L., Maxwell, D. S., and Tirado-Rives, J. (1996) *J. Am. Chem. Soc. 118*, 11225−11236.
35. Qiu, D., Shenkin, P. S., Hollinger, F. P., and Still, W. C. (1997) *J. Phys. Chem. A 101*, 3005−3014.
36. Ponder, J. W., and Richards, F. M. (1987) *J. Comput. Chem. 8*, 1016−1024.
37. Mohamadi, F., Richards, N. G. J., Guida, W. C., Liskamp, R., Lipton, M., Caufield, C., Chang, G., Hendrickson, T., and Still, W. C. (1990) *J. Comput. Chem. 11*, 460−467.
38. Chang, G., Guida, W. C., and Still, W. C. (1989) *J. Am. Chem. Soc. 111*, 4379−4386.
39. Kolossvary, I., and Guida, W. C. (1999) *J. Comput. Chem. 20*, 1671−1684.
40. Xiong, H., Stanley, B. A., Tekwani, B. L., and Pegg, A. E. (1997) *J. Biol. Chem. 272*, 28342−28348.
41. Morris, J. J., and Page, M. I. (1980) *J. Chem. Soc., Perkin Trans. 2*, 685−692.
42. Morris, J. J., and Page, M. I. (1980) *J. Chem. Soc., Perkin Trans. 2*, 679−684.
43. Stanley, B. A., and Pegg, A. E. (1991) *J. Biol. Chem. 266*, 18502−18506.
44. Gunasekaran, K., Gomathi, L., Ramakrishnan, C., Chandrasekhar, J., and Balaram, P. (1998) *J. Mol. Biol. 284*, 1505−1516.
45. Gallagher, T., Rozwarski, D. A., Ernst, S. R., and Hackert, M. L. (1993) *J. Mol. Biol. 230*, 516−528.
46. Parks, E. H., Ernst, S. R., Hamlin, R., Xuong, N. H., and Hackert, M. L. (1985) *J. Mol. Biol. 182*, 455−465.
47. Guan, C., Liu, Y., Shao, Y., Cui, T., Liao, W., Ewel, A., Whitaker, R., and Paulus, H. (1998) *J. Biol. Chem. 273*, 9695−9702.
48. Duan, X., Gimble, F. S., and Quiocho, F. A. (1997) *Cell 89*, 555−564.
49. Mizutani, R., Nogami, S., Kawasaki, M., Ohya, Y., Anraku, Y., and Satow, Y. (2002) *J. Mol. Biol. 316*, 919−929.
50. Poland, B. W., Xu, M. Q., and Quiocho, F. A. (2000) *J. Biol. Chem. 275*, 16408−16413.
51. Esnouf, R. (1997) *J. Mol. Graphics 15*, 132−134.
52. Esnouf, R. M. (1999) *Acta Crystallogr. D55*, 938−940.
53. Merritt, E. A., and Bacon, D. J. (1997) *Methods Enzymol. 277*, 505−524.
54. Kraulis, P. J. (1991) *J. Appl. Crystallogr. 24*, 946−950.

BI0268854